

Higgs-Radion interpretation of the LHC data?

Bohdan Grzadkowski

*Institute of Theoretical Physics,
Faculty of Physics, University of Warsaw,
00-681 Warsaw, Poland*

John F. Gunion

*Department of Physics
University of California, Davis, CA 95616, U.S.A.*

We explore the parameter choices in the five-dimensional Randall-Sundrum model with the inclusion of Higgs-radion mixing that can describe current LHC hints for one or more Higgs boson signals.

I. INTRODUCTION

The two simplest ways of reconciling the weak energy scale $\mathcal{O}(1 \text{ TeV})$ and the much higher GUT or reduced Planck mass scale $\mathcal{O}(10^{18} \text{ GeV})$ in a consistent theory are (i) to employ supersymmetry or (ii) to introduce one or more warped extra dimensions. In this letter, we pursue the 5D version of the latter introduced by Randall and Sundrum (RS) [1], but modified in that all fields other than the Higgs reside in the bulk. Having the gauge and fermion fields in the bulk is needed to adequately suppress flavor changing neutral current (FCNC) operators and operators contributing to precision electroweak (PEW) corrections [2–9].

In the notation of [10], the background RS metric that solves Einstein's equations takes the form

$$ds^2 = e^{-2m_0b_0|y|} \eta_{\mu\nu} dx^\mu dx^\nu - b_0^2 dy^2 \quad (1)$$

where y is the coordinate for the 5th dimension with $|y| \leq 1/2$. The graviton and radion fields, $h_{\mu\nu}(x, y)$ and $\phi_0(x)$, are the quantum fluctuations relative to the background metric $\eta_{\mu\nu}$ and b_0 , respectively. In particular, $\phi_0(x)$ is the quantum degree of freedom associated with fluctuations of the distance between the branes. In the simplest case, only gravity propagates in the bulk while the SM is located on the infrared (or TeV) brane at $y = 1/2$ and the interactions of Kaluza-Klein (KK) gravitons and the radion with the SM are described by

$$\mathcal{L}_{\text{int}} = -\frac{1}{\hat{\Lambda}_W} \sum_{n \neq 0} h_{\mu\nu}^n T^{\mu\nu} - \frac{\phi_0}{\Lambda_\phi} T_\mu^\mu \quad (2)$$

where $h_{\mu\nu}^n(x)$ are the KK modes (with mass m_n) of the graviton field $h_{\mu\nu}(x, y)$. In the above, $\hat{\Lambda}_W \simeq \sqrt{2}m_{Pl}\Omega_0$, where $\Omega_0 = e^{-\frac{1}{2}m_0b_0}$, and $\Lambda_\phi = \sqrt{3}\hat{\Lambda}_W$ is the vacuum expectation value of the radion field. Note from Eq. (2) that the radion couples to matter with coupling strength $1/\Lambda_\phi$. If matter and gauge fields propagate in the bulk then the interactions of gravitons and the radion with the matter and gauge fields are controlled by the overlap of appropriate 5th-dimensional profiles and corrections to Eq. (2) appear.

In addition to the radion, the model contains a conventional Higgs boson, h_0 . The RS model provides a simple solution to the hierarchy problem if the Higgs is placed on the TeV brane at $y = 1/2$ by virtue of the fact that the 4D electro-weak scale v_0 is given in terms of the $\mathcal{O}(m_{Pl})$ 5D Higgs vev, \hat{v} , by:

$$v_0 = \Omega_0 \hat{v} = e^{-\frac{1}{2}m_0b_0} \hat{v} \sim 1 \text{ TeV} \quad \text{for} \quad \frac{1}{2}m_0b_0 \sim 35. \quad (3)$$

As a result, to solve the hierarchy problem, $\Lambda_\phi = \sqrt{6}m_{Pl}\Omega_0$ should be of order $1 - 10 \text{ TeV}$, but not much higher [1].

The ratio m_0/m_{Pl} is a particularly crucial parameter that characterizes the 5-dimensional curvature. As discussed shortly, large curvature values $m_0/m_{Pl} \gtrsim 0.5$ are favored for fitting the LHC Higgs excesses and by bounds on FCNC and PEW constraints. In early discussions of the RS model it was argued that $R_5/M_5^2 < 1$ (M_5 being the 5D Planck scale and $R_5 = 20m_0^2$ the size of the 5D curvature) is needed to suppress higher curvature terms in the 5D action, which leads to $m_0/m_{Pl} \lesssim 0.15$ being preferred. However [9] argues that R_5/Λ^2 (with Λ being the energy scale at which the 5D gravity theory becomes strongly coupled, estimated by naive dimensional analysis to be $\Lambda \sim 2\sqrt{3}\pi M_5$) is the appropriate measure, implying that values as large as $m_0/m_{Pl} < \sqrt{3\pi^3/(5\sqrt{5})} \sim 3$ are acceptable. In this

regard, the relation between the mass of the 1st KK graviton excitation (G^1), m_0/m_{Pl} and Λ_ϕ ,

$$m_1^{\text{KK}} = \frac{(m_0/m_{Pl})x_1^{\text{KK}}}{\sqrt{6}} \Lambda_\phi, \quad (4)$$

where $x_1^{\text{KK}} \sim 3.83$ is the 1st zero of the Bessel function J_1 , will require large m_0/m_{Pl} if the lower bound on m_1^{KK} is large and $\Lambda_\phi \sim 1$ TeV.

In the simplest RS scenario, the SM fermions and gauge bosons are confined to the brane. However, this is now regarded as highly problematical because the higher-dimensional operators in the 5D effective field theory are suppressed only by TeV^{-1} and then FCNC processes and PEW observable corrections are predicted to be much too large. This arrangement also provides no explanation of the flavor hierarchies. It is therefore now regarded as necessary [2–9] to allow all the SM fields (except the Higgs) to propagate in the extra dimension. The SM particles are then the zero-modes of the 5D fields and the profile of a SM fermion in the extra dimension can be adjusted using a mass parameter. If 1st and 2nd generation fermion profiles peak near the Planck brane then FCNC operators and PEW corrections will be suppressed by scales $\gg \text{TeV}$. Even with this arrangement it is estimated that the g^1 , W^1 and Z^1 masses must be larger than about 3 TeV (see the summary in [9]). A second alternative is to use fairly flat profiles for the 1st and 2nd generation fermions in the 5th dimension [11]. In this case, the coupling of light quarks to g^1, W^1, Z^1 , proportional to the integral of the square of the fermion profile multiplied by the gauge boson profile, will be very small, implying small FCNC. PEW constraints would still be very problematical unless a special 5D GIM mechanism is employed [12]. In either case, the interactions of Eq. (2) are greatly modified when gauge bosons and fermions are allowed to propagate in the bulk,

If the gauge bosons and fermions do not propagate in the bulk, then the strongest limits on Λ_ϕ come, via Eq. (4), from the lower bound placed by the LHC on the first graviton KK excitation (see, for example, [13] and [14] for the ATLAS and CMS limits). However, when the fermions propagate in the bulk, the couplings of light fermion pairs to G^1 are greatly reduced and these limits do not apply. When gauge bosons propagate in the bulk, a potentially important experimental limit on the model comes from lower bounds on the 1st excitation of the gluon, g^1 . In the model of [15], in which light fermion profiles peak near the Planck brane, there is a universal component to the light quark coupling $q\bar{q}g^1$ that is roughly equal to the SM coupling g times a factor of ζ^{-1} , where $\zeta \sim \sqrt{\frac{1}{2}m_0b_0} \sim 5 - 6$. The suppression is due to the fact that the light quarks are localized near the Planck brane whereas the KK gluon is localized near the TeV brane. Even with such suppression, the LHC g^1 production rate due to $u\bar{u}$ and $d\bar{d}$ collisions is large. Further, whatever the model, the $t_R\bar{t}_Rg^1$ coupling is large since the t_R profile peaks near the TeV brane – the prediction of [15] is $g_{t_R\bar{t}_Rg^1} \sim \zeta g$. As a result, the dominant decay of the g^1 is to $t\bar{t}$. ATLAS and CMS search for $t\bar{t}$ resonances at high mass. Using $g_{q\bar{q}g^1} \sim g/5$, $q = u, d$, one finds a lower bound of $m_1^g \gtrsim 1.5$ TeV [16] using an update of the analysis of [15]. ([17] gives a weaker bound of $m_1^g > 0.84$ TeV.)

In terms of Λ_ϕ , we have the following relations:

$$\frac{m_0}{m_{Pl}} = \frac{\sqrt{6}}{x_1^g} \frac{m_1^g}{\Lambda_\phi} \simeq \frac{m_1^g}{\Lambda_\phi}, \quad \text{and} \quad \frac{1}{2}m_0b_0 = -\log\left(\frac{\Lambda_\phi}{\sqrt{6}m_{Pl}}\right) \quad (5)$$

where $x_1^g = 2.45$ is the 1st zero of an appropriate Bessel function. If the model really solves the hierarchy problem then $\hat{\Lambda}_W$ cannot be much larger than 1 TeV. Let us take $\hat{\Lambda}_W \lesssim 5.5$ TeV as an extreme possibility, which implies $\Lambda_\phi = \sqrt{3}\hat{\Lambda}_W \lesssim 10$ TeV. If we adopt the CMS limit of $m_1^g > 1.5$ TeV then Eq. (5) implies a lower limit on the 5-dimensional curvature of $m_0/m_{Pl} \gtrsim 0.15$. Thus, a significant lower bound on m_1^g implies that only relatively large values for m_0/m_{Pl} are allowed. As discussed above, m_0/m_{Pl} values up to $\sim 2 - 3$ are probably consistent with curvature corrections to the RS scenario being small. Still, tension between the lower bound on m_1^g and keeping acceptably small m_0/m_{Pl} could increase to an unacceptable point as the LHC data set increases. We will discuss the phenomenology that applies if the value of Λ_ϕ for any given (m_0/m_{Pl}) is tied to the lower bound of $m_1^g = 1.5$ TeV using Eq. (5). Alterations to the phenomenology using $m_1^g = 3$ TeV, as perhaps preferred by PEW constraints, will also be illustrated.

However, there are alternative approaches in which the lower bound on m_1^g from the LHC can be much smaller. If the g^1 , W^1 and Z^1 are light then precision electroweak and FCNC constraints will be violated unless light quarks do not couple to them, as would be the case if the light fermion profiles are flat. In this case, an experimental lower bound on m_1^g could not be obtained using the techniques employed so far. However, it is worth noting that if $\Lambda_\phi = 1$ TeV is desired, then for $m_0/m_{Pl} = 0.01, 0.1$ Eq. (5) implies $m_1^g = 10, 100$ GeV, respectively. Could the g^1 really have escaped discovery for such low masses? In this extreme, one needs to analyze LHC rates for $gg \rightarrow gg^1$ ($gg \rightarrow g^1$ vanishes as a result of Yang's theorem) using diagrams involving a top-quark loop. The enhanced $t_R\bar{t}_Rg^1$

coupling could overcome the one-loop factor and lead to a large g^1 production rate and a limit rather similar to what is obtained in the model of Ref. [15]. A detailed analysis is needed. If it is assumed that there is no firm bound on m_1^g it then becomes appropriate to discuss the phenomenology that arises for fixed Λ_ϕ . This will be discussed for $\Lambda_\phi = 1$ TeV and 1.5 TeV.

Since the radion and Higgs fields have the same quantum numbers, it is generically possible to introduce kinetic mixing between them. The mixing action can be written in the form: [18]

$$S_\xi = \xi \int d^4x \sqrt{g_{\text{vis}}} R(g_{\text{vis}}) \hat{H}^\dagger \hat{H}, \quad (6)$$

where $R(g_{\text{vis}})$ is the Ricci scalar for the metric induced on the visible brane, and \hat{H} is the Higgs field in the 5-D context before rescaling to canonical normalization. The physical mass eigenstates, h and ϕ , are obtained by diagonalizing and canonically normalizing the kinetic (and mass) terms in the Higgs-radion Lagrangian. The diagonalization procedures and results for the h and ϕ using our notation can be found in [10] (see also [18, 19]).¹ In the end, one finds

$$h_0 = dh + c\phi \quad -\phi_0 = a\phi + bh, \quad \text{where} \quad d = \cos \theta - t \sin \theta, \quad c = \sin \theta + t \cos \theta, \quad a = -\frac{\cos \theta}{Z}, \quad b = \frac{\sin \theta}{Z}, \quad (7)$$

with $t = 6\xi\gamma/Z$, $Z^2 = 1 + 6\xi\gamma^2(1 - 6\xi)$ and $\tan 2\theta = 12\gamma\xi Z m_{h_0}^2 / (m_{\phi_0}^2 [Z^2 - 36\xi^2\gamma^2])$. Here $m_{h_0}^2$ and $m_{\phi_0}^2$ are the Higgs and radion masses before mixing. Consistency of the diagonalization imposes strong restrictions on the possible ξ values as a function of the final eigenstate masses m_h and m_ϕ , which restrictions depend strongly on the ratio $\gamma \equiv v_0/\Lambda_\phi$ ($v_0 = 246$ GeV).

The full Feynman rules after mixing for the h and ϕ interactions with gauge bosons and fermions located in the bulk were derived in [20]. Of particular note are the anomaly terms associated with the ϕ_0 interactions before mixing. To be precise, we give a few details of these important couplings and their implications. Let us begin by defining

$$g_h = (d + \gamma b) \quad g_\phi = (c + \gamma a) \quad g_h^r = \gamma b \quad g_\phi^r = \gamma a. \quad (8)$$

Relative to the Feynman rules of Fig. 29 of [10], the following modifications of the gg and $\gamma\gamma$ couplings are required when the gauge bosons propagate in the bulk:

$$\begin{aligned} c_g^{h,\phi} &= -\frac{\alpha_s}{4\pi v} \left[g_{h,\phi} \sum_i F_{1/2}(\tau_i) - 2(b_3 + \frac{2\pi}{\alpha_s \frac{1}{2} m_0 b_0}) g_{h,\phi}^r \right] \\ c_\gamma^{h,\phi} &= -\frac{\alpha}{2\pi v} \left[g_{h,\phi} \sum_i e_i^2 N_c^i F_i(\tau_i) - (b_2 + b_Y + \frac{2\pi}{\alpha \frac{1}{2} m_0 b_0}) g_{h,\phi}^r \right] \end{aligned} \quad (9)$$

(In Fig. 29 of [10] we used the notation g_{fV} for what we here call $g_{h,\phi}$. Also g_r from [10] is replaced here by $g_{h,\phi}^r$ which incorporates the bulk propagation effects by the virtue of the second term in the parenthesis above.) Since $b_3 = 7$ and $b_2 + b_Y = -11/3$, the new g^r corrections can be significant.

There are also modifications to the WW and ZZ couplings of the h and ϕ relative to Fig. 29 of [10]. Without bulk propagation, these couplings were simply given by SM couplings (proportional to the metric tensor $\eta^{\mu\nu}$) times g_h or g_ϕ . For the bulk propagation case, there are additional terms in the interaction Lagrangian that lead to Feynman rules that have terms not proportional to $\eta^{\mu\nu}$, see [20]. For example, for the W we have (before mixing)

$$\mathcal{L} \ni h_0 \frac{2m_W^2}{v} W_\mu^\dagger W^\mu - \phi_0 \frac{2m_W^2}{\Lambda_\phi} \left[W_\mu^\dagger W^\mu (1 - \kappa_W) + W_{\mu\nu}^\dagger W^{\mu\nu} \frac{1}{4m_W^2 (\frac{1}{2} m_0 b_0)} \right] \quad (10)$$

where $\kappa_V = \left(\frac{3m_V^2 (\frac{1}{2} m_0 b_0)}{\Lambda_\phi^2 (m_0/m_{Pl})^2} \right)$ for $V = W, Z$. After mixing, this becomes, for example for the h interaction

$$\mathcal{L} \ni h \frac{2m_W^2}{v} \left[g_h^W W_\mu^\dagger W^\mu + g_h^r \frac{1}{4m_W^2 (\frac{1}{2} m_0 b_0)} W_{\mu\nu}^\dagger W^{\mu\nu} \right] \equiv h \frac{2m_W^2}{v} g_h^W [W_\mu^\dagger W^\mu + \eta_h^W W_{\mu\nu}^\dagger W^{\mu\nu}] \quad (11)$$

¹ In the current paper we change the sign of our convention for ϕ_0 . We also note that in [18, 19] the coefficients in the h_0 decomposition are denoted by a, b and those in the ϕ_0 decomposition are denoted c, d , *i.e.* the reverse of our conventions.

with a similar result for the ϕ . Here we have defined

$$g_{h,\phi}^V \equiv g_{h,\phi} - g_{h,\phi}^r \kappa_V, \quad \eta_{h,\phi}^V \equiv \frac{g_{h,\phi}^r}{g_{h,\phi}^V} \frac{1}{4m_V^2(\frac{1}{2}m_0 b_0)}. \quad (12)$$

Substituting one $m_W = \frac{1}{2}gv$ this gives the Feynman rule for the hWW coupling as

$$igm_W g_h^W [\eta_{\mu\nu}(1 - 2k^+ \cdot k^- \eta_h^W) + 2\eta_h^W k_\mu^+ k_\nu^-] \quad (13)$$

where k^+, k^- are the momenta of the W^+, W^- , respectively. The notations and results for the ϕ and for $V = Z$ are obtained by corresponding modifications. Now, defining $R_{h,\phi}^V = 2\eta_{h,\phi}^V m_V^2 / (1 - 2k^+ \cdot k^- \eta_{h,\phi}^V)$ and $x_V^{h,\phi} \equiv 4m_V^2 / m_{h,\phi}^2$, one finds that the matrix-element-squared for $h, \phi \rightarrow VV$ is proportional to

$$(g_{h,\phi}^V)^2 (1 - 2k^+ \cdot k^- \eta_{h,\phi}^V)^2 \left\{ \left[1 - x_V^{h,\phi} + \frac{3}{4}(x_V^{h,\phi})^2 \right] + R_{h,\phi}^V \left[-6 + \frac{4}{x_V^{h,\phi}} + 2x_V^{h,\phi} \right] + (R_{h,\phi}^V)^2 \left[4 + \frac{4}{(x_V^{h,\phi})^2} - \frac{8}{x_V^{h,\phi}} \right] \right\}, \quad (14)$$

where $k^+ \cdot k^- = (2m_V^2 / x_V^{h,\phi})(1 - \frac{1}{2}x_V^{h,\phi})$. The SM result would be obtained by setting $g_{h,\phi}^V = 1$ and $\eta_{h,\phi}^V = 0$.

For the fermions, we assume profiles such that there are no corrections to the h_0 and ϕ_0 couplings due to propagation in the bulk. This is a very good approximation for the top quark quark which must be localized near the TeV brane. Also for the bottom quark the approximation is better than 20%, see [20]. Even though the approximation is not necessarily good for light quarks, it is only the heavy quarks that impact the phenomenology of the Higgs-radion system.

Our goal in this paper is to illustrate the complexity of the phenomenology of the Higgs-radion system in the context of LHC data. We will show in particular that an approximate fit to the most prominent “excesses” in the Higgs search data can be explained in the context of the model. Earlier papers on this topic include [21], [22] (see also [23]) and [24].

II. LHC EXCESSES

The Large Hadron Collider (LHC) data from the ATLAS [25] and CMS [26] collaborations suggests the possibility of a fairly Standard Model (SM) like Higgs boson with mass of order 123 – 128 GeV. In particular, promising hints appear of a narrow excess over background in the $\gamma\gamma$ and $ZZ \rightarrow 4\ell$ final states with strong supporting evidence from the $WW \rightarrow \ell\nu\ell\nu$ mode. The ATLAS results suggest that the $\gamma\gamma$ and 4ℓ rates may be significantly enhanced with respect to the SM expectation at a mass near 125 GeV. The CMS $\gamma\gamma$ rate is maximal for $M_{\gamma\gamma} \sim 124$ GeV and also appears to be somewhat enhanced with respect to the SM expectation. At this mass the CMS signals in other channels, including $\ell\nu\ell\nu$ and 4ℓ are roughly consistent with the expectation for a SM Higgs. In addition, CMS data shows excesses in the 4ℓ rate near 120 GeV (at which mass they do not see a $\gamma\gamma$ excess) and in the $\gamma\gamma$ rates near 137 GeV (at which mass there is no 4ℓ excess), but neither is confirmed in the ATLAS data.

One important point regards the $W^+W^- \rightarrow \ell\nu\ell\nu$ final state. The signal for a scalar state of any given mass will be spread out into many bins of a variable such as the transverse mass, m_T , as a result of the missing energy carried by the neutrinos. Thus, if there are two scalar states that have equal production cross section times WW branching ratio both may contribute but their contribution will depend upon the analysis cuts applied. This contrasts with the $ZZ \rightarrow 4\ell$ channel (the only ZZ channel analyzed for scalar masses below 200 GeV) and the $\gamma\gamma$ channel both of which have excellent mass resolution so that excesses should appear centered on the scalar state masses. For this reason, we focus on these latter channels.

In the context of the Higgs-radion model, positive signals can only arise for two masses. If more than two excesses were to ultimately emerge, then a more complicated Higgs sector will be required than the single h_0 case we study here. Certainly, one can consider including extra Higgs singlets or doublets. For the moment, we presume that there are at most two excesses. In this case, it is sufficient to pursue the single Higgs plus radion model.

We will consider three cases, labelled as ATLAS, CMSA and CMSB. We quantify the excesses in terms of the best fit value for $R(X) \equiv \sigma(X)/\sigma_{\text{SM}}(X)$ for a given final state X . Errors quoted for the excesses are those for $\pm 1\sigma$. The mass locations and excesses in the $\gamma\gamma$ and 4ℓ channels in these three cases are taken from Figs. 8a and 8b of [25] in the ATLAS case and from the appropriate windows of Fig. 14 of [26] in the case of CMSA and CMSB:

1. ATLAS:

125 GeV: $\gamma\gamma$ excess of $R(\gamma\gamma) = 2_{-0.8}^{+0.8}$;

125 GeV: 4ℓ excess of $R(4\ell) = .5_{-1}^{+1.5}$;

No significant excesses at any other mass.

2. CMSA:

124 GeV: $\gamma\gamma$ excess of $R(\gamma\gamma) = 1.7^{+0.8}_{-0.7}$;
 124 GeV: 4ℓ excess of $R(4\ell) = 0.5^{+1.1}_{-0.7}$;
 120 GeV: 4ℓ excess of $R(4l) = 2^{+1.5}_{-1}$ but $R(\gamma\gamma) < 0.5$.

3. CMSB:

124 GeV: as for CMSA;
 137 GeV: $R(\gamma\gamma) = 1.5^{+0.8}_{-0.8}$;
 137 GeV: $R(4\ell) < 0.2$.

To an excellent approximation, only the gg initial state is relevant for h and ϕ production followed by decay to $\gamma\gamma$ or $ZZ \rightarrow 4\ell$ and so we will be comparing the ratios

$$R_h(X) \equiv \frac{\Gamma_h(gg)\text{BR}(h \rightarrow X)}{\Gamma_{h_{SM}}(gg)\text{BR}(h_{SM} \rightarrow X)}, \quad R_\phi(X) \equiv \frac{\Gamma_\phi(gg)\text{BR}(\phi \rightarrow X)}{\Gamma_{h_{SM}}(gg)\text{BR}(h_{SM} \rightarrow X)}, \quad (15)$$

where numerator and denominator are computed for the same mass, to the ATLAS, CMSA and CMSB $R(X)$ values quoted above. We also note that CMS gives results for $W, Z + b\bar{b}$ relative to $W, Z + h_{SM}$ with $h_{SM} \rightarrow b\bar{b}$ in the SM at 120 GeV and 124 GeV of $1^{+1.4}_{-1.4}$ and $0.5^{+1.3}_{-1.5}$, respectively. No measurement for the $b\bar{b}$ final state is quoted for 137 GeV.

We note that the error bars on the SM multipliers for the ATLAS, CMSA and CMSB scenarios are large and we regard it as likely that the central values will surely change with more integrated luminosity at the LHC. Increased integrated luminosity will hopefully increase the agreement between the ATLAS and CMS excesses, but could also worsen the consistency, or perhaps even lead to the disappearance of the excesses. Thus, the comparisons below should only be taken as illustrative of the possibilities. (Note that our plots are always done with either m_h or m_ϕ equal to 125 GeV as appropriate for the ATLAS excess. However, there is no change in the plots if we use 124 GeV, as more precisely appropriate to the central value of the CMSA and CMSB excesses.)

As discussed above, it is appropriate to consider two different kinds of models: one in which a strong lower bound on the masses of the first excitations of the gauge bosons applies and one in which the fermionic profiles are such that the bounds on the gauge boson excitations are very weak. We consider these two alternatives in turn.

A. Lower bound on m_1^g

In this section, we consider a model along the lines of [15] in which FCNC and PEW constraints are satisfied by virtue of the fermionic profiles being peaked fairly close to the Planck brane leading to fairly definitive couplings of the fermions to the excited gauge bosons. As described earlier, a lower bound of $m_1^g \sim 1.5$ TeV can be obtained from LHC data while FCNC and PEW constraints suggest a still higher bound of ~ 3 TeV. We will show some results for both choices as we step through various possible mass locations for the Higgs and radion that are motivated by the LHC excesses in the $\gamma\gamma$ and/or 4ℓ channels. In what follows, each plot will be labelled by the value of m_0/m_{Pl} chosen and the corresponding $m_{Pl}\Omega_0$ value as calculated for the fixed m_1^g using Eq. (5).

1. Signal at only 125 GeV

In Fig. 1 we illustrate some possibilities for $m_h = 125$ GeV and $m_\phi = 120$ GeV taking $m_1^g = 1.5$ TeV. First, we note that to get an enhanced $\gamma\gamma$ rate at 125 GeV, it is necessary to have $m_0/m_{Pl} \gtrsim 0.4$ and $\xi < 0$. In order to have small $R_\phi(\gamma\gamma)$ and $R_\phi(4\ell)$ at 120 GeV while at the same time $R_h(\gamma\gamma) \gtrsim 1.5$ at 125 GeV, for consistency with the ATLAS scenario, then $m_0/m_{Pl} = 0.4$ and $\xi \sim -0.09$ are good choices. The somewhat larger associated value of $R_h(4\ell)$ is still consistent within errors with the ATLAS observation at 125 GeV. We note that for the reversed assignments of $m_h = 120$ GeV and $m_\phi = 125$ GeV, we cannot find parameter choices that yield a decent description of the ATLAS 125 GeV excesses with $R_h(\gamma\gamma)$ and $R_h(4\ell)$ being sufficiently suppressed at 120 GeV.

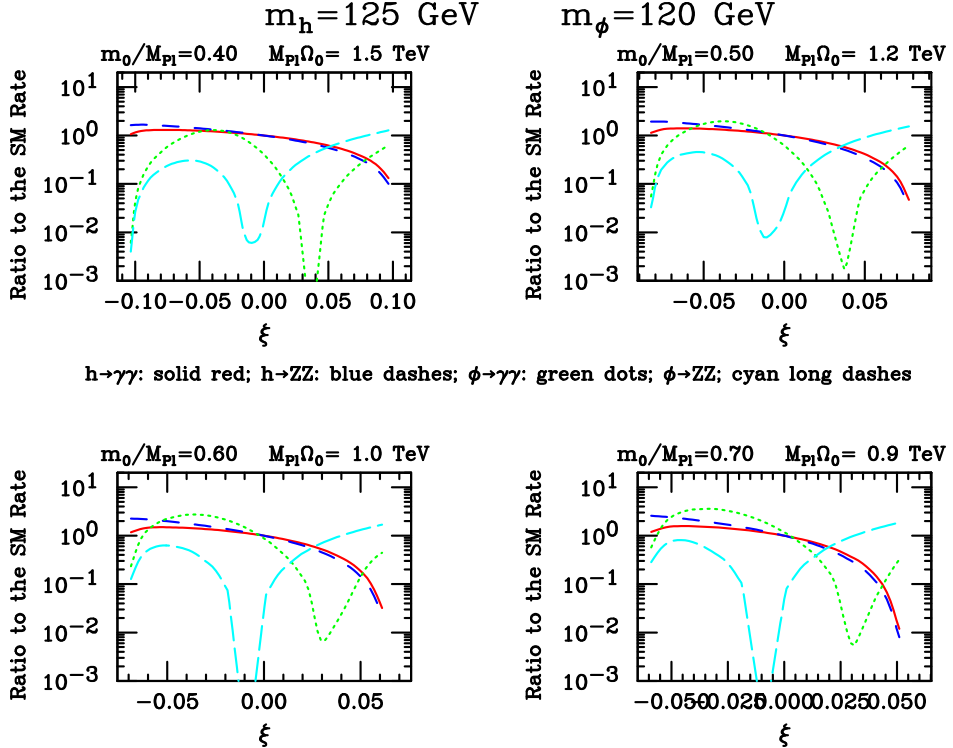


FIG. 1: For $m_h = 125$ GeV and $m_\phi = 120$ GeV, we plot $R_h(X)$ and $R_\phi(X)$ for $X = \gamma\gamma$ and $X = ZZ$ (equivalent to $X = 4\ell$) as a function of ξ , assuming $m_1^g = 1.5$ TeV.

2. Signals at 125 GeV and 120 GeV

Fig. 1 also exemplifies the fact that with $m_1^g = 1.5$ TeV the Higgs-radion model is unable to describe the CMSA scenario. In the regions of ξ for which appropriate signals are present at 125 GeV from the h , then at 120 GeV the 4ℓ and $\gamma\gamma$ rates are either both suppressed or $R_\phi(\gamma\gamma) > R_\phi(4\ell)$. This phenomenon persists at higher m_0/m_{Pl} values as well as higher m_1^g .

3. Signals at 125 GeV and 137 GeV

Let us next consider the CMSB scenario, *i.e.* neglecting the 4ℓ excess at 120 GeV in the CMS data. In Fig. 2 we see that the choices $m_0/m_{Pl} = 0.5$ and $\xi = 0.12$ give $R_h(\gamma\gamma) \sim 1.3$ and $R_h(4\ell) \sim 1.5$ at 125 GeV and $R_\phi(\gamma\gamma) \sim 1.3$ at 137 GeV, fairly consistent with the CMSB observations. However, $R_\phi(4\ell) \sim 0.5$ at 137 GeV is a bit too large. Also shown in the figure are the rates for $Z, W + h$ with $h \rightarrow b\bar{b}$ and $Z, W + \phi$ with $\phi \rightarrow b\bar{b}$ relative to their SM counterparts. For the above $m_0/m_{Pl} = 0.5$, $\xi = 0.12$ choices, the $Z, W + h(\rightarrow b\bar{b})$ rate at 125 GeV is only slightly below the SM value, whereas the $Z, W + \phi(\rightarrow b\bar{b})$ rate is about 10% of the SM level predicted at 137 GeV. The former is consistent with the poorly measured $b\bar{b}$ rate at 124 GeV while confirmation of the latter would require much more integrated luminosity.

We also note that it is not possible to get enhanced $\gamma\gamma$ and $4\ell h$ signals at 125 GeV without having visible 137 GeV ϕ signals, *i.e.* the ATLAS scenario of no observable excesses other than those at 125 GeV cannot be realized for $m_\phi = 137$ GeV.

For this case, it is also interesting to consider results for $m_h = 125$ GeV and $m_\phi = 137$ GeV for the higher value of $m_1^g = 3$ TeV. Results for this choice are plotted in Fig. 3. We observe that $R_h(\gamma\gamma)$ and $R_h(4\ell)$ are both $\lesssim 1$ (or less) except for $m_0/m_{Pl} = 0.7$ and large ξ for which $R_\phi(\gamma\gamma) \ll 1$. Thus, a reasonable description of the CMSB scenario requires relatively small m_1^g .

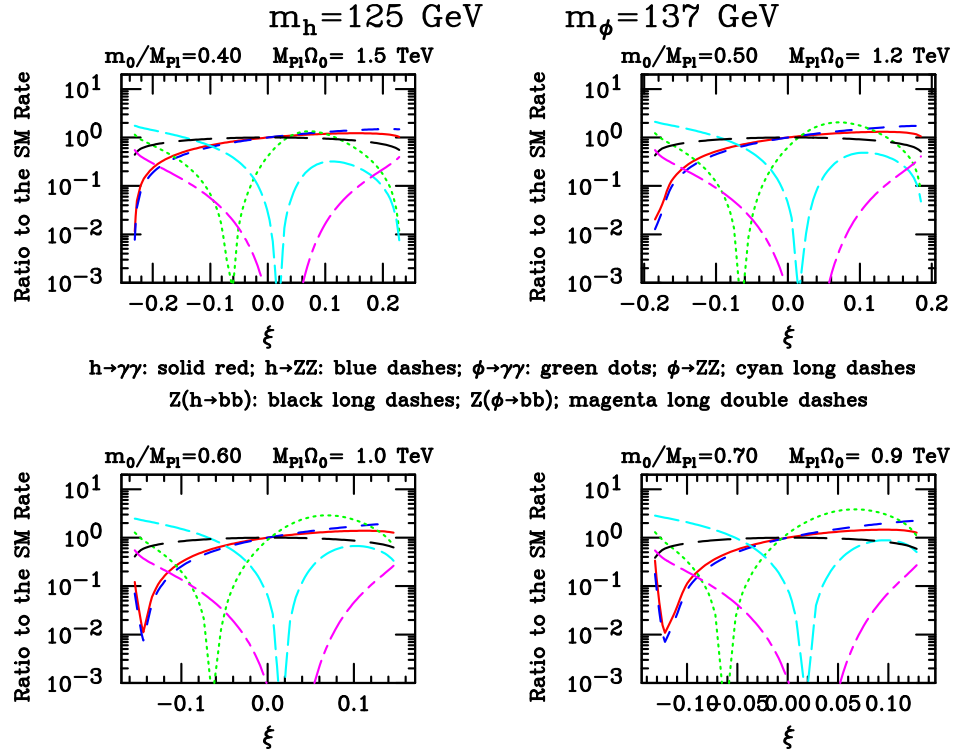


FIG. 2: For $m_h = 125$ GeV and $m_\phi = 137$ GeV, we plot $R_h(X)$ and $R_\phi(X)$ for $X = \gamma\gamma$ and $X = ZZ$ (equivalent to $X = 4\ell$) as a function of ξ , assuming $m_1^g = 1.5$ TeV. Also shown are the similarly defined ratios for $Z + h$ production with $h \rightarrow b\bar{b}$ and $Z + \phi$ production with $\phi \rightarrow b\bar{b}$.

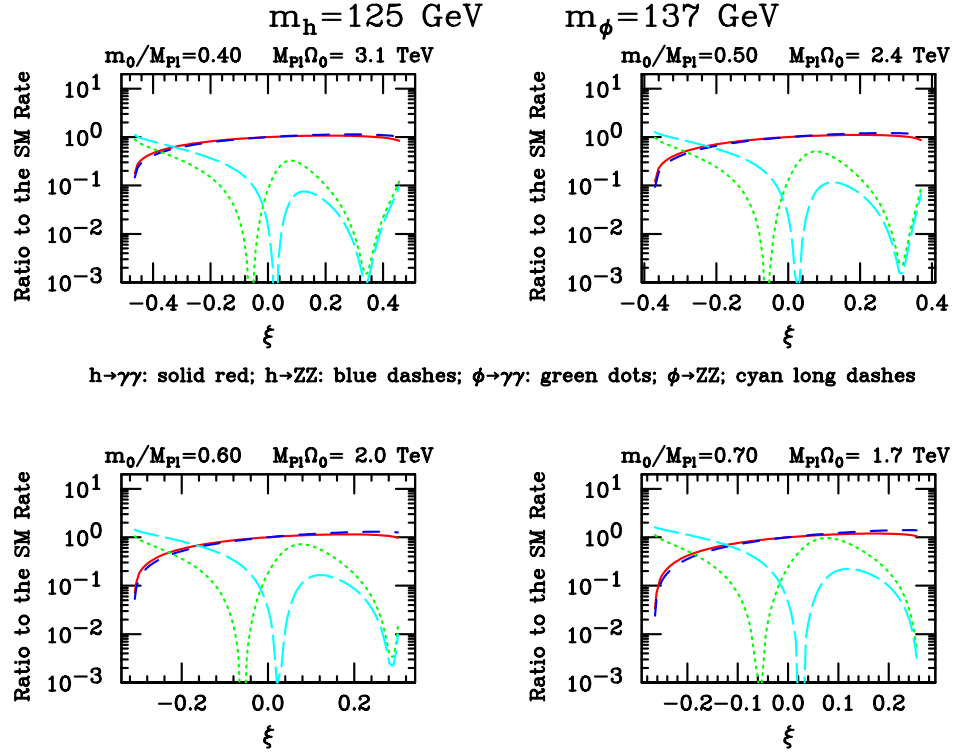


FIG. 3: For $m_h = 125$ GeV and $m_\phi = 137$ GeV, we plot $R_h(X)$ and $R_\phi(X)$ for $X = \gamma\gamma$ and $X = ZZ$ (equivalent to $X = 4\ell$) as a function of ξ , assuming $m_1^g = 3$ TeV.

4. Signals at 125 GeV and high mass

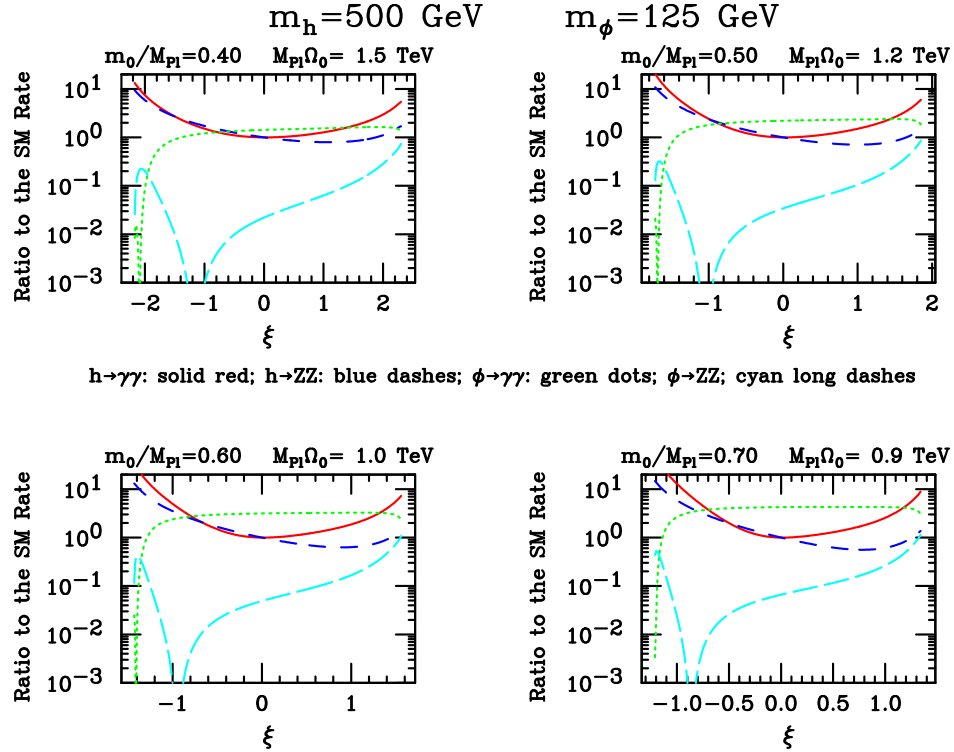


FIG. 4: For $m_h = 500$ GeV and $m_\phi = 125$ GeV, we plot $R_h(X)$ and $R_\phi(X)$ for $X = \gamma\gamma$ and $X = ZZ$ (equivalent to $X = 4\ell$) as a function of ξ , assuming $m_1^g = 1.5$ TeV.

A general question is whether one could explain the ATLAS 125 GeV excesses as being due to the h or ϕ with the other being at high mass. If $m_h = 125$ GeV and $m_\phi > 500$ GeV, one finds that $R_h(\gamma\gamma) \sim R_h(4\ell) \sim 1$ for ξ above some minimum (negative) value, with values substantially below 1 for more negative ξ . In any case, precision electroweak constraints are violated if $|\xi|$ is not quite modest in size since at large $|\xi|$ the ϕVV ($V = W, Z$) couplings become of SM strength or larger. For more discussion see [27].

If the mass assignments are reversed, $m_\phi = 125$ GeV and $m_h > 500$ GeV, then at the most positive ξ values one can achieve $R_\phi(\gamma\gamma) \sim 2$ and $R_\phi(4\ell) \sim 1$ at 125 GeV for $m_0/m_{Pl} = 0.4$ and 0.5 , as shown in Fig. 4 for the example of $m_h = 500$ GeV. However, this scenario is even less consistent with precision electroweak constraints since for all ξ the h alone has hVV couplings that are at least SM-like. Much larger Λ_ϕ would be needed to have a hope of achieving PEW consistency [27] and for large Λ_ϕ ATLAS-like $>SM$ signals at $m_h = 125$ GeV would not be achievable. In addition, the $h \rightarrow 4\ell$ signal at high mass would be at least as large as predicted for a high-mass SM-like Higgs and therefore quite observable if $m_h \lesssim 500$ GeV, as seemingly inconsistent with ATLAS and CMS data. If $m_h \sim 1$ TeV, then the 4ℓ signal would be beyond current LHC reach but PEW inconsistency would be much worse. Thus, we conclude that for the Higgs-radion model to be of interest, both m_h and m_ϕ should be modest in size.

B. Fixed Λ_ϕ

In this section, we consider the second type of model discussed in the introduction in which the fermionic profiles are quite flat and the couplings of light quarks to the gauge excitations are therefore very small. This is a situation that has not been studied with regard to LHC constraints. Thus, we feel free to consider the rather low values of Λ_ϕ ,

$\Lambda_\phi = 1$ TeV and $\Lambda_\phi = 1.5$ TeV, for which the Higgs-radion model can yield LHC rates in the $\gamma\gamma$ and 4ℓ channels that exceed those that are predicted for a SM Higgs. We note that when the gauge bosons propagate in the bulk, the phenomenology does not depend on Λ_ϕ alone — at fixed Λ_ϕ explicit plots not given here show that there is strong dependence on m_0/m_{Pl} when m_0/m_{Pl} is small. However, for large $m_0/m_{Pl} \gtrsim 0.5$ the phenomenology is determined almost entirely by Λ_ϕ , but is still not the same as found in the case where all fields are on the TeV brane. Once again, we step through the various possible mass locations for the Higgs and radion that are motivated by the LHC excesses in the $\gamma\gamma$ and/or 4ℓ channels.

1. Signal only at 125 GeV

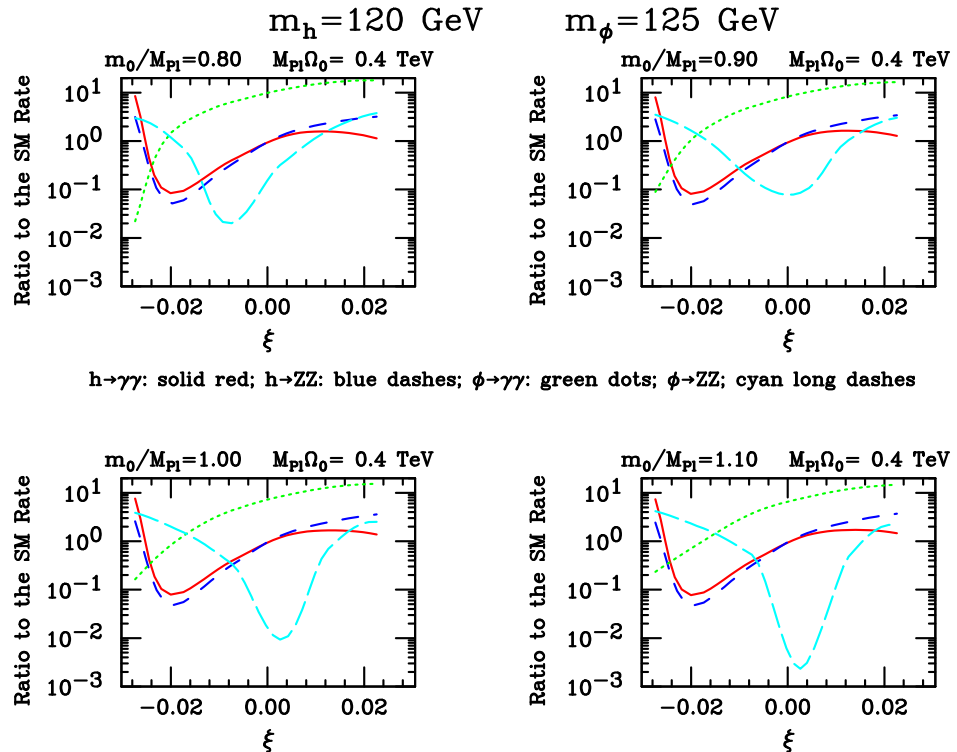


FIG. 5: For $m_h = 120$ GeV and $m_\phi = 125$ GeV, we plot $R_h(X)$ and $R_\phi(X)$ for $X = \gamma\gamma$ and $X = ZZ$ (equivalent to $X = 4\ell$) as a function of ξ taking Λ_ϕ fixed at 1 TeV.

As shown in Fig. 5, the choice of $\Lambda_\phi = 1$ TeV with $m_\phi = 125$ GeV and $m_h = 120$ GeV gives a reasonable description of the ATLAS excesses at 125 GeV with no visible signals at 120 GeV in either the $\gamma\gamma$ or 4ℓ channels when one chooses $m_0/m_{Pl} = 1$ and $\xi = -0.016$. In contrast, for $\Lambda_\phi = 1.5$ TeV the 125 GeV predicted excesses are below $1 \times \text{SM}$ and thus would not provide a good description of the ATLAS data. As exemplified in Fig. 6, for the reversed assignments of $m_h = 125$ GeV and $m_\phi = 120$ GeV any choice of parameters that gives a good description of the 125 GeV signals always yields a highly observable 120 GeV signal.

2. Signals at 125 GeV and 120 GeV

We can also consider Fig. 6 to see if there is a choice of ξ for which consistency with the CMSA scenario is achieved. We observe that if ξ is at its maximum value and $m_0/m_{Pl} = 1.1$ then the $\gamma\gamma$ and 4ℓ signals at $m_h = 125$ GeV are

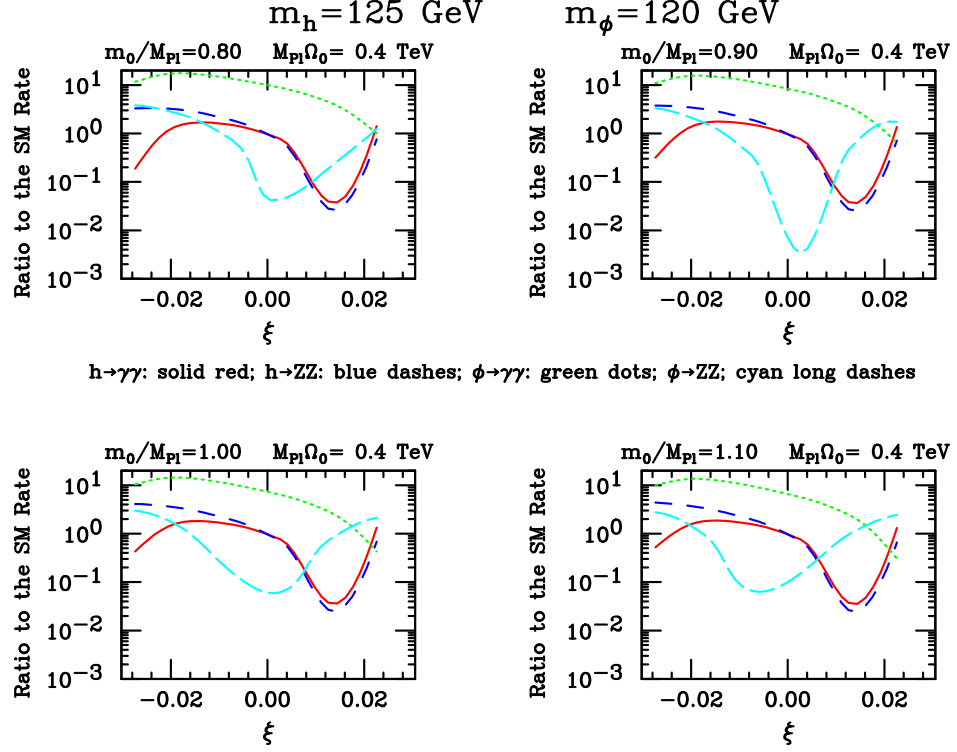


FIG. 6: For $m_h = 125$ GeV and $m_\phi = 120$ GeV, we plot $R_h(X)$ and $R_\phi(X)$ for $X = \gamma\gamma$ and $X = ZZ$ (equivalent to $X = 4\ell$) as a function of ξ taking Λ_ϕ fixed at 1 TeV.

still within -1σ of the CMS data while at $m_\phi = 120$ GeV one finds $R_\phi(4\ell) \sim 2.5$ while $R_\phi(\gamma\gamma) \sim 0.3$, which values are roughly consistent with the CMSA situation. For the reversed assignments of $m_h = 120$ GeV and $m_\phi = 125$ GeV, Fig 5 illustrates the fact that a satisfactory description of the two CMSA excesses is not possible — for ξ such that appropriate 125 GeV excesses are present, $R_h(\gamma\gamma)$ and $R_h(4\ell)$ at 120 GeV are always small so that the 4ℓ excess at 120 GeV is not explained.

3. Signals at 125 GeV and 137 GeV

Let us now consider the CMSB scenario. For $\Lambda_\phi = 1$ TeV, one finds $m_h = 125$ GeV and $m_\phi = 137$ GeV with the choices $m_0/m_{Pl} = 0.6$ and $\xi = -0.05$ give $R_h(\gamma\gamma) \sim 2$ and $R_h(4\ell) \sim 1$ at 125 GeV, while $R_\phi(\gamma\gamma) \sim 2$ and $R_\phi(4\ell) \sim 0.4$ at 137 GeV, an ok description of the CMSB excesses. An equally rough description of this same situation is also possible for $\Lambda_\phi = 1$ TeV with $m_0/m_{Pl} = 0.8$ and $\xi = 0.05$.

For $\Lambda_\phi = 1.5$ TeV a somewhat better simultaneous description of these excesses is possible. Fig. 7 shows some results for $m_h = 125$ GeV and $m_\phi = 137$ GeV. For $m_0/m_{Pl} = 0.25$ and $\xi \sim -0.1$ one finds $R_h(\gamma\gamma) \sim 2$ and $R_h(4\ell) \sim 1.5$ at $m_h = 125$ GeV, while $R_\phi(\gamma\gamma) \sim 2$ and $R_\phi(4\ell) \ll 1$ at $m_\phi = 137$ GeV, in pretty good agreement with the CMSB scenario.

If we reverse the configuration to $m_h = 137$ GeV and $m_\phi = 125$ GeV, the only parameter choices that come close to describing the two excess are $\Lambda_\phi = 1$ TeV with $m_0/m_{Pl} = 0.8$ and $\xi \sim 0.05$ for which one finds that the $m_\phi = 125$ GeV $\gamma\gamma$ and 4ℓ signals and the $m_h = 137$ GeV $\gamma\gamma$ signal are all at the level of $\sim 1.4 \times \text{SM}$. However, the $m_h = 137$ GeV 4ℓ signal is at the level of $\sim 0.6 \times \text{SM}$ which is 4σ away from the CMS central value at this mass. For these mass assignments, the higher $\Lambda_\phi = 1.5$ TeV value does not provide any parameter choices that come close to describing the CMS excesses — the $m_\phi = 125$ GeV signals are never both sufficiently large *at the same time* to fit the observed

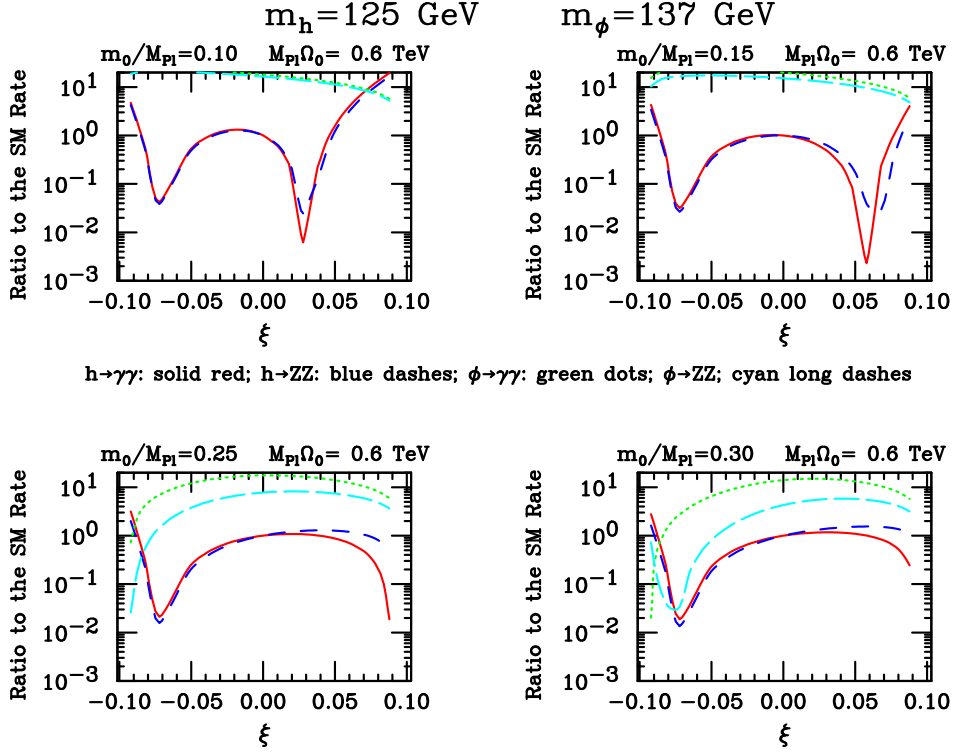


FIG. 7: For $m_h = 125$ GeV and $m_\phi = 137$ GeV, we plot $R_h(X)$ and $R_\phi(X)$ for $X = \gamma\gamma$ and $X = ZZ$ (equivalent to $X = 4\ell$) as a function of ξ taking Λ_ϕ fixed at 1.5 TeV.

signals.

4. Signals at 125 GeV and higher mass

We choose not to show any specific plots for this situation. For $\Lambda_\phi = 1$ TeV or 1.5 TeV, it is possible to choose one of either the h or ϕ to have a mass of 125 GeV and find m_0/m_{Pl} and ξ values that result in a decent description of the 125 GeV ATLAS excesses. However, these scenarios always are such as to imply a large inconsistency with PEW constraints and, if the higher mass is chosen below 500 GeV, a highly observable 4ℓ signal that would be inconsistent with ATLAS and CMS observations in that region of mass.

5. SM Higgs at 125 GeV and Signal at 137 GeV

It is still quite conceivable that, after accumulating more data, the excesses at ~ 125 GeV will converge to those appropriate for a SM Higgs boson. Such a situation would correspond to taking $\xi = 0$ in the Higgs-radion model. In this case, one can ask whether or not there could be a radion at some nearby mass and what its experimental signature would be. To exemplify, let us suppose that the signal at 137 GeV of the CMSB scenario survives. In Fig. 8 we plot $R_h(X)$ and $R_\phi(X)$ for $X = \gamma\gamma$ and $X = 4\ell$ as a function of Λ_ϕ for a selection of m_0/m_{Pl} values, taking $\xi = 0$. One observes that a nice description of the $R(\gamma\gamma) \sim 2$ excess at 137 GeV is possible, for example, for $m_0/m_{Pl} = 0.3$ at $\Lambda_\phi \sim 2.8$ TeV with the 4ℓ signal being very suppressed. As also apparent, other choices of the m_0/m_{Pl} and Λ_ϕ will also yield $R_\phi(\gamma\gamma) \sim 2$ with varying levels of 4ℓ and $b\bar{b}$ signals. (However, to suppress $R_\phi(4\ell)$ below 0.2 while achieving $R_\phi(\gamma\gamma) \sim 2$ requires $m_0/m_{Pl} \geq 0.3$.) We also note that for $\xi = 0$ the $Z, W + \phi \rightarrow b\bar{b}$ is greatly suppressed

relative to its SM counterpart due to the very suppressed $ZZ\phi$ coupling.

Plots for the case of a SM Higgs at 125 GeV and $m_\phi = 120$ GeV look very similar and, in particular, it is not possible to find parameters for which the 4ℓ signal substantially exceeds the $\gamma\gamma$ signal — the reverse always applies, as one anticipates from the enhanced anomalous $\gamma\gamma$ coupling of the (unmixed) ϕ .

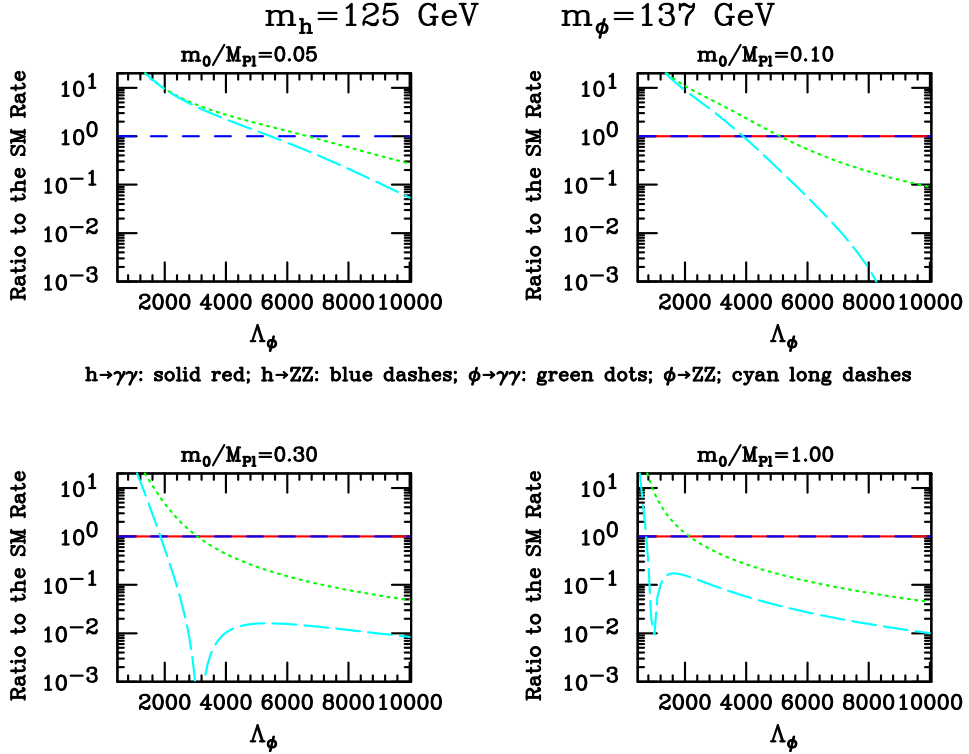


FIG. 8: For $m_h = 125$ GeV and $m_\phi = 137$ GeV, we plot $R_h(X)$ and $R_\phi(X)$ for $X = \gamma\gamma$ and $X = ZZ$ (equivalent to $X = 4\ell$) as functions of Λ_ϕ taking $\xi = 0$.

III. SUMMARY AND CONCLUSIONS

The Randall Sundrum model solution to the hierarchy problem yields interesting phenomenology for the Higgs-radion sector, especially when Higgs-radion mixing is allowed for, and can be made consistent with FCNC and PEW constraints if fermions and gauge bosons propagate in the 5th dimension. At the moment, there are interesting hints at the LHC of narrow excesses above SM backgrounds in the $\gamma\gamma$ and $ZZ \rightarrow 4\ell$ channels, as well as a broad excess in the $WW \rightarrow \ell\nu\ell\nu$ channel. ATLAS sees excesses in the $\gamma\gamma$ and 4ℓ channels at a mass of ~ 125 GeV of order $2 \times \text{SM}$ and $1.5 \times \text{SM}$ respectively. CMS sees a $\gamma\gamma$ excess of order $1.5 \times \text{SM}$ at ~ 124 GeV and constrains the 4ℓ channel at this mass to be less than $\sim 1.5 \times \text{SM}$. Additional excesses at 120 GeV (in the 4ℓ channel) and at 137 GeV (in the $\gamma\gamma$ channel) are present in the CMS data.

In this paper, we explored a wide range of possibilities within the Randall Sundrum model context. In a first set of plots, we correlated Λ_ϕ (the radion field vacuum expectation value) with the curvature ratio m_0/m_{Pl} assuming that there was a lower bound on the mass of the 1st excited gluon state of order 1.5 TeV, as estimated using LHC data in the class of scenarios in which the 5th dimension profiles for light fermions need to be peaked near the Planck brane in order to avoid corrections to FCNC and PEW constraints that are too large.

However, not all modeling allows such a strong bound on the g^1 mass to be derived using LHC data or FCNC and PEW constraints. In particular, if the light fermion profiles are quite flat, the production rate for the g^1 at the LHC is very small and, further, most FCNC and PEW constraints are satisfied for rather low masses for the g^1, W^1, Z^1

provided appropriate symmetries are introduced. Our second set of plots are done holding Λ_ϕ fixed at either 1 TeV or 1.5 TeV.

Since the single Higgs plus radion model can describe at most two Higgs-like excesses, we considered three scenarios labelled as: ATLAS, with $\gamma\gamma$ and 4ℓ excesses at 125 GeV larger than SM and no other significant excesses; CMSA, with $\gamma\gamma$ and 4ℓ excesses at 124 GeV above SM level and a 4ℓ excess at 120 GeV; and, CMSB, with $\gamma\gamma$ and 4ℓ excesses at 124 GeV above those predicted for a SM Higgs boson of this same mass along with a $\gamma\gamma$ excess at 137 GeV that is also larger than would have been predicted for $m_{h_{SM}} = 137$ GeV. In both the fixed m_1^g and the fixed Λ_ϕ model possibilities, the signal levels of the ATLAS and CMSB scenarios could be nicely described, whereas a satisfactory description of the CMSA case was not found. In general, successful fitting of the ATLAS and CMSB excesses required a modest value for the radion vacuum expectation value, $\Lambda_\phi \lesssim 2$ TeV, and $m_0/m_{Pl} \gtrsim 0.5$, a range that the most recent discussion suggests is still consistent with higher curvature corrections to the RS scenario being small.

We also considered expectations for the radion signal in the case where the Higgs signal was assumed to ultimately converge to precisely that for a SM Higgs of mass 125 GeV. This situation would arise if the there is no Higgs-radion mixing. We found that interesting excesses at the radion mass would be present for low enough Λ_ϕ , namely $\Lambda_\phi \lesssim 3$ TeV, but would always be characterized by a $\gamma\gamma$ signal that substantially exceeds the 4ℓ signal (as appropriate for the CMS excesses at 137 GeV but in definite contradiction with the CMS excesses at 120 GeV).

Acknowledgments

The authors thank Kaustubh Agashe, Felix Brummer, Csaba Csaki, Gero Von Gersdorff, Tom Rizzo and John Terning for illuminating discussions on radion physics.

This work has been partially financed by the National Science Centre (Poland) as a research project, decision no DEC-2011/01/B/ST2/00438. JFG is supported by US DOE grant DE-FG03-91ER40674.

[1] L. Randall and R. Sundrum, Phys. Rev. Lett. **83** (1999) 3370 [arXiv:hep-ph/9905221];
[2] H. Davoudiasl, J. L. Hewett and T. G. Rizzo, Phys. Lett. B **473**, 43 (2000) [hep-ph/9911262].
[3] A. Pomarol, Phys. Lett. B **486**, 153 (2000) [hep-ph/9911294].
[4] T. Gherghetta, A. Pomarol, Nucl. Phys. **B586**, 141-162 (2000). [hep-ph/0003129].
[5] H. Davoudiasl, J. L. Hewett, T. G. Rizzo, Phys. Rev. **D63**, 075004 (2001). [hep-ph/0006041].
[6] C. Csaki, J. Erlich and J. Terning, Phys. Rev. D **66**, 064021 (2002) [hep-ph/0203034].
[7] J. L. Hewett, F. J. Petriello and T. G. Rizzo, JHEP **0209**, 030 (2002) [hep-ph/0203091].
[8] K. Agashe, A. Delgado, M. J. May and R. Sundrum, JHEP **0308**, 050 (2003) [hep-ph/0308036].
[9] K. Agashe, H. Davoudiasl, G. Perez and A. Soni, Phys. Rev. D **76**, 036006 (2007) [hep-ph/0701186].
[10] D. Dominici, B. Grzadkowski, J. F. Gunion and M. Toharia, Nucl. Phys. B **671**, 243 (2003) [arXiv:hep-ph/0206192]; Acta Phys. Polon. B **33**, 2507 (2002) [arXiv:hep-ph/0206197].
[11] G. Cacciapaglia, C. Csaki, C. Grojean and J. Terning, Phys. Rev. D **71**, 035015 (2005) [hep-ph/0409126].
[12] G. Cacciapaglia, C. Csaki, J. Galloway, G. Marandella, J. Terning and A. Weiler, JHEP **0804**, 006 (2008) [arXiv:0709.1714 [hep-ph]].
[13] G. Aad *et al.* [ATLAS Collaboration], arXiv:1112.2194 [hep-ex].
[14] S. Chatrchyan *et al.* [CMS Collaboration], arXiv:1112.0688 [hep-ex].
[15] K. Agashe, A. Belyaev, T. Krupovnickas, G. Perez and J. Virzi, Phys. Rev. D **77**, 015003 (2008) [hep-ph/0612015].
[16] S. Rappoccio [CMS Collaboration], arXiv:1110.1055 [hep-ex].
[17] The ATLAS Collaboration, ATLAS-CONF-2011-123.
[18] G. F. Giudice, R. Rattazzi and J. D. Wells, Nucl. Phys. B **595**, 250 (2001) [arXiv:hep-ph/0002178].
[19] J. L. Hewett and T. G. Rizzo, JHEP **0308**, 028 (2003) [hep-ph/0202155].
[20] C. Csaki, J. Hubisz, S. J. Lee, Phys. Rev. **D76**, 125015 (2007). [arXiv:0705.3844 [hep-ph]].
[21] H. de Sandes, R. Rosenfeld, [arXiv:1111.2006 [hep-ph]].
[22] V. Barger, M. Ishida, [arXiv:1110.6452 [hep-ph]].
[23] V. Barger, M. Ishida and W. -Y. Keung, arXiv:1111.4473 [hep-ph].
[24] K. Cheung and T. -C. Yuan, arXiv:1112.4146 [hep-ph].
[25] ATLAS Collaboration, ATLAS-CONF-2011-163.
[26] CMS Collaboration, CMS-PAS-HIG-11-032.
[27] J. F. Gunion, M. Toharia and J. D. Wells, Phys. Lett. B **585**, 295 (2004) [hep-ph/0311219].